Original Article

Technology in Cancer Research & Treatment
Volume 22: 1-10

DOI: 10.1177/15330338221147122
journals.sagepub.com/home/tct

Assessment of Hepatic Lesions After non-Thermal Tumor Ablation by Irreversible Electroporation in a Pig Model

Sung-Min Jeon, PhD[1,3], Enkhzaya Davaa, PhD[1], Yixin Jiang, PhD[1,2,3], Ratchapol Jenjob, PhD[1,2], Ngoc-Thuan Truong, Ms[1,2], Kyung-Ju Shin, PhD[1,2], Seok Jeong, MD, PhD[4], and Su-Geun Yang, PhD[1,2,3]

Abstract

Irreversible electroporation (IRE) is a non-thermal and minimal invasive modality to ablate pathologic lesions such as hepatic tumors. Histological analysis of the initial lesions after IRE can help predict ablation efficacy. We aimed to investigate the histological characteristics of early hepatic lesions after IRE application using animal models. IRE (1500 V/cm, a pulse length of 100 μs, 60 or 90 pulses) was applied to the liver of miniature pigs. H&E and TUNEL staining were performed and analyzed. Ablated zones of pig liver were discolored and separated from the normal zone after IRE. Histologic characteristics of ablation zones included preserved hepatic lobular architecture with a unique hexagonal-like structure. Apoptotic cells were detected, and sinusoidal dilatation and blood congestion were observed, but hepatic arteries and bile ducts were intact around the ablation zones. The early lesions obtained by delivering monophasic square wave pulses through needle electrodes reflected typical histological changes induced by IRE. Therefore, it was found that the histological assessment of the early hepatic lesion after IRE can be utilized to predict the IRE ablation effect.

Keywords

ablation zones, histological characteristic, liver, irreversible electroporation (IRE), needle electrodes

Abbreviations

CRT, capillary refill time; DBP, diastolic blood pressure; HCC, hepatocellular carcinoma; H&E, hematoxylin and eosin; IRE, irreversible electroporation; MBP, mean arterial pressure; MWA, microwave ablation; MM, mucous membrane color; PA, percutaneous ablation; RFA, radiofrequency ablation; SBP, systolic blood pressure; SpO_2, saturation of partial pressure oxygen; TUNEL, Terminal deoxynucleotidyl transferase-mediated dUTP digoxigenin nick end labeling.

Received: June 28, 2022; Revised: November 7, 2022; Accepted: November 30, 2022.

[1] Department of Biomedical Science, Translational Research center, Inha University Hospital, Incheon, Korea
[2] Department of Biomedical Science, BK21 FOUR Program in Biomedical Science and Engineering, Inha University College of Medicine, Incheon, Korea
[3] Inha Institute of Aerospace Medicine, Inha University College of Medicine, Incheon, Korea
[4] Division of Gastroenterology, Inha University Hospital, Inha University College of Medicine, Incheon, Korea

Corresponding Authors:
Su-Geun Yang, Department of Biomedical Science, Inha University College of Medicine, 366 Seohae-Daero Jung-Gu, Incheon 22332, Korea.
Email: sugeun.yang@inha.ac.kr

Seok Jeong, Division of Gastroenterology, Inha University Hospital, Inha University College of Medicine, 27 Inhang-ro, Jung-Gu, Incheon 22332, Korea.
Email: inos@inha.ac.kr

Introduction

Percutaneous ablation (PA), along with surgical resection of the tumor and liver transplantation, have been recommended as curative treatments for hepatocellular carcinoma (HCC).[1] PA is a minimally invasive tissue ablation modality, which includes thermal ablations, such as radiofrequency ablation (RFA) and microwave ablation (MWA), and nonthermal irreversible electroporation (IRE).[1] In particular, IRE has the advantage of a short treatment period compared to conventional hyperthermal ablation modalities.[2] IRE ablates the target tissue by applying short pulse length (nanosecond to millisecond length) and high-amplitude electric pulses.[1,3–5]

Two or more needle electrodes are mainly used for IRE ablation,[2] and the pulsed electric fields generated through the electrodes form permanent nanopores in the cell membrane of the target tissue. The nanopores cause the loss of cellular homeostasis (eg, cytoskeleton destabilization and ATP depletion) as well as the loss of osmotic effects, eventually leading to cell death.[3,4,6–8] There are four cell death types initiated by electroporation-based ablation (apoptosis, pyroptosis, necroptosis, and necrosis), and these types may differ within the treatment zone, by target cell types, or electric field strength.[9]

A representative premature sign of cell apoptosis or necrosis detected in the early phase of IRE ablation is the infiltration of erythrocytes into the widened hepatic sinusoids of the treated zone.[5,10,11] Along with sinusoidal dilatation and sinusoidal congestion, important histological characteristics due to unique nonthermal IRE were found in the IRE ablation zone. Critical tubular structures (eg, nerves, hepatic arteries, bile ducts, and other major blood vessels) were preserved intact in the ablation zone even after IRE treatment.[10,11] IRE is also insensitive to the heat sink effect of the surrounding blood flow, does not cause vessel occlusion, and induces activation of the immune system.[1,4,12] Therefore, IRE is considered a useful ablation modality for hepatic malignancies adjacent to where thermal ablation is contraindicated, such as the bile tract, blood vessels, or portal vein.[3,6] Despite the advantages of IRE ablation described above, it was reported that IRE electrical pulses induced involuntary muscle contractions, required general anesthesia, or sometimes might induce cardiac arrhythmia.[4,6,7,13,14] Few published studies have reported on the changed properties of liver tissues during the early phase of IRE ablation. Moreover, few studies have described the distribution of apoptotic regions in the hepatic lobule in the initial lesion of IRE ablation.

Histological analysis of the initial lesion after IRE helps predict the ablation efficacy according to IRE conditions. Therefore, we investigated the histological characteristics of the initial lesion in detail including the distribution analysis of the apoptotic areas in the hepatic lobule after IRE on the liver of miniature pigs using needle-types electrodes.

Materials and Methods

Animals

The current study was performed with the approval (KNOTUS IACUC: 21-KE-441) of the Institutional Animal Care and Use Committee of KNOTUS Co. Ltd (Incheon, Korea). Two healthy male miniature pigs (Jeju-native *Sus scrofa* domesticus, average body weight 26.6 ± 0.3 kg, Cronex. Co. Ltd, Hwaseong, Korea) were used for the electroporation study using needle electrodes. Animals were housed and acclimated in the housing room of KNOTUS Co. Ltd for 7 days under the following conditions: temperature of $23°C \pm 3°C$; relative humidity $55\% \pm 15\%$; ventilation frequency of 10~20 times/h; 12-h light/dark cycle (lights on 08:00 AM); luminous intensity of 150~300 Lux. Food (Cargill Agri Purina, Inc, Gyeonggi-do, Korea) was provided to the animals (500 g each), and water was freely ingested using an automatic water supply device. General anesthesia was induced by the intramuscular injection of alfaxalone (3 mg/kg), and intraoperative anesthesia was maintained by the inhalation of 1.5%–2% isoflurane. Tramadol (3 mg/kg) was injected intravenously to minimize the animal's pain before the IRE application. Animal vital signs and ventilation status were monitored using anesthesia workstations (Dräger Fabius® Plus, Drägerwerk AG & Co., Germany) (Figure C). A midline laparotomy was performed to expose the hepatic lobe. The reporting of animal study followed the ARRIVE 2.0 guidelines.[15]

In Vivo IRE Procedure for Porcine Liver

The IRE procedure was performed according to the approved experimental protocol (KNOTUS IACUC: 21-KE-441). A prototype needle-type electrode was used to investigate the histopathological characteristics of livers treated with IRE. Needle electrodes were fabricated in the laboratory using acupuncture needles with closed conical stainless steel active tips (21-gauge, 8 cm length), a polyolefin insulating sheath, and a rigid plastic electrode spacer (Figure 1A and 1B). The proximal portion of the electrodes was connected to a direct current pulse generator (ECM 830 square wave electroporation system, BTX Genetronics, CA, USA). Monophasic square wave pulses (electric field intensity of 1500 V/cm, a pulse length of 100 μs, 60 or 90 pulses, 10 mm-electrode active tip length) were delivered to the porcine hepatic lobe via a pair of monopolar needle electrodes (Figure 1D). The above procedure was applied to both pigs, but was performed sequentially for each animal to avoid confusion about animal tissue sampling after IRE.

Monitoring for Vital Signs and Muscle Contraction

Vital signs of miniature pigs were monitored before and after the application of IRE (Figure 1C). Seven vital signs were monitored as follows: blood pressure (systolic pressure, diastolic pressure, mean arterial pressure, mm Hg), heart rate (beats/min), respiratory rate (breaths/ min), rectal temperature (°C), saturation of partial pressure oxygen (SpO_2, %), capillary refill time (CRT), and mucous membrane color (MM). The occurrence and number of muscle contractions during IRE were visually analyzed based on live image recordings taken with a mobile phone camera (Galaxy S10 5G, Samsung Electronics Co., Ltd, Korea).

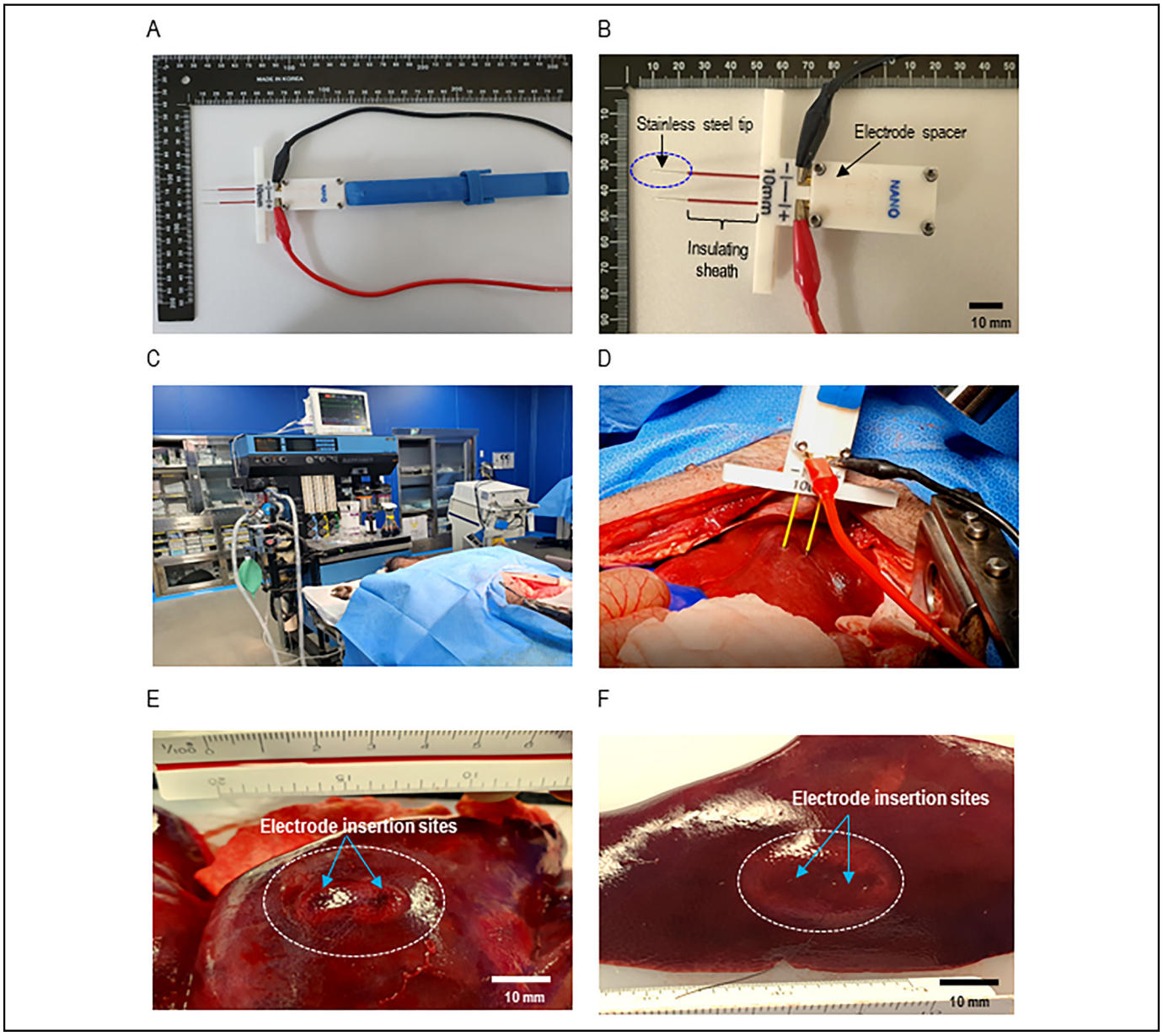

Figure 1. Photographs showing the IRE electrode configuration, animal monitoring system, and morphology of the IRE ablation zone formed in the liver of a miniature pig model. (A) Laboratory-fabricated needle type electrodes were used in this study. A pair of acupunctures, pulse generator connecting cables, and an electrode holder were assembled on the electrode spacer. (B) Major assembly portion of needle electrodes consisting of a closed conical stainless steel active tip, polyolefin insulating sheath, and a rigid plastic electrode spacer. (C) Anesthesia system and vital sign monitoring devices. (D) Delivery of monophasic square-wave pulses to the liver tissue. (E) Dumbbell-shaped elliptical ablation zone in the hepatic lobe after 90 pulses. The discolored elliptical ablation zone (located within the white dashed circle) formed around the electrode insertion site (blue arrow). (F) Oval elliptical ablation zone in the hepatic lobe after 60 pulses.

Macroscopic and Histological Examination of IRE Ablation Zone

The pigs were deeply anesthetized with 5% *isoflurane* and sacrificed by exsanguinations within 2 h after IRE application. The ablated tissue samples were harvested for histological analysis of early hepatic lesions. The overall shape of the ablation zone was observed grossly, and the long and short axes of the zone were measured using digital vernier calipers (Mitutoyo Co., Kawasaki, Japan). To observe the microstructure within the IRE ablation zone, the tissue sections (thickness of 4 μm) were stained with hematoxylin and eosin (H&E). Terminal deoxynucleotidyl transferase-mediated dUTP digoxigenin nick end labeling (TUNEL) staining was also performed with diaminobenzidine (G7130, Promega, USA) according to the manufacturer's protocol. To investigate the dilatation of hepatic sinusoids by IRE, 20 equal-sized image fields were

Table 1. Comparison of Vital Signs Before and After IRE of the Hepatic Lobes of Miniature Pigs.

Pig name	Hepatic lobe sample name	Voltage (V)	Pulse length (μs)	Pulse number (pulses)	IRE treatment	Blood pressure (SBP/DBP/MBP, mm Hg)	Heart rate (beats/min)	Respiratory rate (breaths/min)	Rectal temperature (°C)	SpO_2 (%)	CRT	MM
Pig 1	P1-L1	1500	100	90	Before	132/88/103	124	10	35.8	96	< 2 s	pink
					After	132/112/119	168	10	35.4	82	< 2 s	pink
Pig 1	P1-L2	1500	100	60	Before	128/86/100	130	10	35.8	98	< 2 s	pink
					After	138/102/114	180	10	36.0	81	< 2 s	pink
Pig 2	P2-L1	1500	100	90	Before	128/86/100	129	10	34.4	86	< 2 s	pink
					After	132/88/103	138	10	34.5	85	< 2 s	pink
Pig 2	P2-L2	1500	100	60	Before	134/86/102	136	10	34.4	89	< 2 s	pink
					After	136/86/103	140	10	34.5	88	< 2 s	pink

SBP, systolic blood pressure; DBP, diastolic blood pressure; MBP, mean arterial pressure; SpO_2, saturation of partial pressure oxygen; CRT, capillary refill time; MM, mucous membrane color; SPO_2.

randomly selected from untreated control and IRE-treated tissue sections. The sinusoidal diameter of each image field was measured using Image J software 1.52a (NIH, USA)

Statistical Analysis

A nonparametric one-way ANOVA was used to compare the difference in sinusoidal diameter between groups in untreated control, IRE 60 pulses, and IRE 90 pulses. The data are expressed as the median and interquartile range. A p-value less than 0.05 ($n = 20$) was considered significant. Data were analyzed with GraphPad Prism software, version 7.0 (GraphPad Software Inc., La Jolla, CA, USA).

Results

Changes in Animal Vital Signs Before and After Irreversible Electroporation

We compared vital signs before and after IRE to the hepatic lobes in two miniature pigs (Table 1). No significant changes in the respiratory rate, CRT, MM, and rectal temperature before and after IRE were in both pig 1 and pig 2. However, the heart rate and blood pressure were significantly increased and the SpO_2 was decreased in pig1 after IRE. There were no significant changes in the blood pressure and SpO_2, but an increase in the heart rate was observed in pig 2 after IRE. Live images showed that involuntary muscle contractions occurred as many as the number of IRE input pulses (60 or 90) during IRE pulse delivery in both pigs (Table 2).

Macroscopic Changes in Porcine Liver Tissue After IRE

We investigated the ablation characteristics after IRE application to the hepatic lobes at fixed electric field intensity of 1500 V/cm (Table 2 and Figure 2). The color of the hepatic parenchyma surrounding the electrode insertion points turned from dark red to pale red after IRE, whereas the dark red color was maintained in tissue areas not affected by IRE (Figure 1E and 1F). The basic shape of the ablation zone formed by needle electrodes was elliptical, and the overall shape was slightly different according to the hepatic lobes or pulse numbers. The area of discolored elliptical tissue including the electrode insertion point (blue arrow) was defined as the ablation area. A dumbbell-shaped ablation zone with a clear margin was observed in hepatic lobes treated with 90 pulses (Figure 1E). The margin sharpness of the ablation zone was lower in the lobes treated with 60 pulses than with 90 pulses (Figure 1E and 1F). The size of the surface ablation zone was larger after 60 pulses than with 90 pulses (Table 2). The ablation zone size after 90 pulses was 19 mm in length and 12 mm in width. The ablation zone after 60 pulses was 20–21 mm in length and 16 mm in width. On the whole slide image, no tissue damage was observed in the untreated parenchyma (Figure 2A), whereas an elliptical ablation zone (black dashed line) was observed in the IRE-treated parenchyma (Figure 2B).

Histologic Characteristics of IRE Ablation Boundaries

The sharpness of the ablation boundary (white dotted line) between the ablation zone and the unaffected zone was partially clear in hepatic parenchyma treated with 90 IRE pulses (Figure 2C). Remarkable intrahepatic bleeding was observed within the ablation zone, unlike the unaffected normal zone by H&E-staining (Figure 2D). The TUNEL stained image indicated the ablation boundary between the dark brown stained apoptotic area and unaffected normal area was also partially clear even in the tissue treated with 60 pulses (Figure 2E and 2F).

Distribution Pattern of IRE-Induced Apoptotic Cells Within Hepatic Lobule Unit

Microscopic image analysis revealed that the unique hexagonal-like structure was preserved in the hepatic lobules despite stimulation at an electric field intensity of 1500 V/cm (Figure 2I and 2K). We further investigated the distribution characteristics of apoptotic cells inside hepatic lobule units or between hepatic lobules after IRE application. Apoptotic cells with a dark

Table 2. Ablation Zone Characteristics in Hepatic Lobes After IRE Application and Generation of Muscle Contraction During IRE Pulse Delivery at a Fixed Electric Field Intensity of 1500 V/cm.

Pig name	Hepatic lobe sample name	Pulse number (pulses)	Surface ablation zone size		Overall shape of ablation zone	Muscle contraction during IRE
			Length (mm)	Width (mm)		
Pig 1	P1-L1	90	19	12	Elliptical	+
Pig 1	P1-L2	60	21	16	Oval elliptical	+
Pig 2	P2-L1	90	19	12	Dumbbell-shaped elliptical	+
Pig 2	P2-L2	60	20	16	Oval elliptical	+

+: generation of muscle contraction.

brown color coexisted with live cells in the hepatic lobules of the IRE ablation zone (Figure 2I). Most of the apoptotic cells were partially connected to adjacent hepatic lobules and live and apoptotic cells were randomly distributed at the center or margins within the hepatic lobule unit (Figure 2I and 2J). Some apoptotic cells were independently distributed in adjacent hepatic lobules, and these apoptotic cells were mainly distributed slightly inward compared with the outermost margin of one hepatic lobule unit, whereas the live cells were mainly distributed at the margins of the hepatic lobules (Figure 2K and 2L).

Sinusoidal Dilatation in IRE-Ablated Liver Tissues

The radial distribution of dilated sinusoids around the hepatic lobular central vein (CV) was observed in both tissues treated with 60 and 90 pulses (Figure 3A and 3B) and the sinusoid was filled with erythrocytes (Figure 3D). The dilated sinusoids were predominantly distributed on the inward portion rather than on the margin of the hepatic lobule of the apoptotic zone (Figure 3C). The sinusoid diameters within the IRE ablation zone were dilated approximately twofold greater than those of the untreated zone (9.5 ± 1.5 μm) (Figure 3E). However, there was no significant difference in sinusoidal diameter between the hepatic parenchyma treated with two different IRE pulses (20.6 ± 2.0 μm for 60 pulses and 19.2 ± 2.8 μm for 90 pulses, respectively).

Sinusoidal Congestion and Bleeding in the Hepatic Parenchyma After IRE

Intrahepatic hemorrhage occurred in IRE-treated hepatic parenchyma (Figure 3G-K), unlike untreated hepatic parenchyma (Figure 3F). Extensive congestion was found in some liver lobules treated with 90 pulses (Figure 3H) but not in lobules treated with 60 pulses (Figure 3G). Sinusoidal congestion, in which blood cells had infiltrated into the widened sinusoid, was also identified in the hepatic parenchyma treated with IRE (Figure 3J and 3K).

Intact Preservation of Tubular Structures in IRE Ablation Zones

Typical cross-sectional structures of the hepatic artery (black arrow) and bile duct (white arrow) were observed in the ablation zone with sinusoidal congestion after 60 (Figure 4A-C) or 90 IRE pulses (Figure 4D and 4E). The structures of hepatic arteries and bile ducts were also preserved in the tissues treated with IRE, and blood cells were inside the hepatic arteries (Figure 4B and 4E). No signs of IRE-applied tubular structural destruction were detected in the tissue sections stained with TUNEL (Figure 4C and 4F). Bile duct structures and cells surrounding the bile duct within the apoptotic areas were not stained dark brown by TUNEL staining (Figure 4C and 4F, white arrow). Although it was an ablation zone, live cells were predominantly distributed in the periphery adjacent to the preserved hepatic artery and bile duct.

Discussion

One of the advantages of IRE that was highlighted was its use for thermal ablation of contraindicated lesions.[3,16–18] In many preclinical studies using normal or tumor-bearing animal models, IRE experiments were performed with electric field strengths of 1,000–2,500 V/cm for effective tissue destruction.[2] In addition, although the range of IRE input parameters applied preclinically and clinically vary, they mainly deliver pulses to the tissue under the conditions of field strength of 1500 V/cm, a pulse length of 50–100 μs, 8–90 pulses, and frequency of 1 Hz.[4,8,10,11,19] In this study, the IRE input parameters (1500 V/cm, pulse length 100 μs, 60 or 90 pulses, 1 Hz) were expected to have an effective IRE ablation effect and were set for the IRE conditions described above. To predict the safety and effectiveness of IRE under these conditions, vital signs before and after IRE using needle electrodes were compared in a general miniature pig model, and histological characteristics of early liver lesions were identified. Advantages of IRE include short ablation time, avoidance of heat or cooling effects, preservation of vital structures within the IRE ablation zone, induction of apoptotic cell death, and complete ablation by a well-demarcated IRE.[14] However, IRE is a pulse-type electrical stimulation that can induce pulse-related muscle contractions and was reported to induce cardiac arrhythmias.[4,7,13,14] Muscle contractions were accompanied by each pulse delivered to the hepatic lobes of two pigs. The heart rate was the most sensitive factor to IRE stimulation in miniature pigs among the seven vital signs. The heart rate levels tended to rise

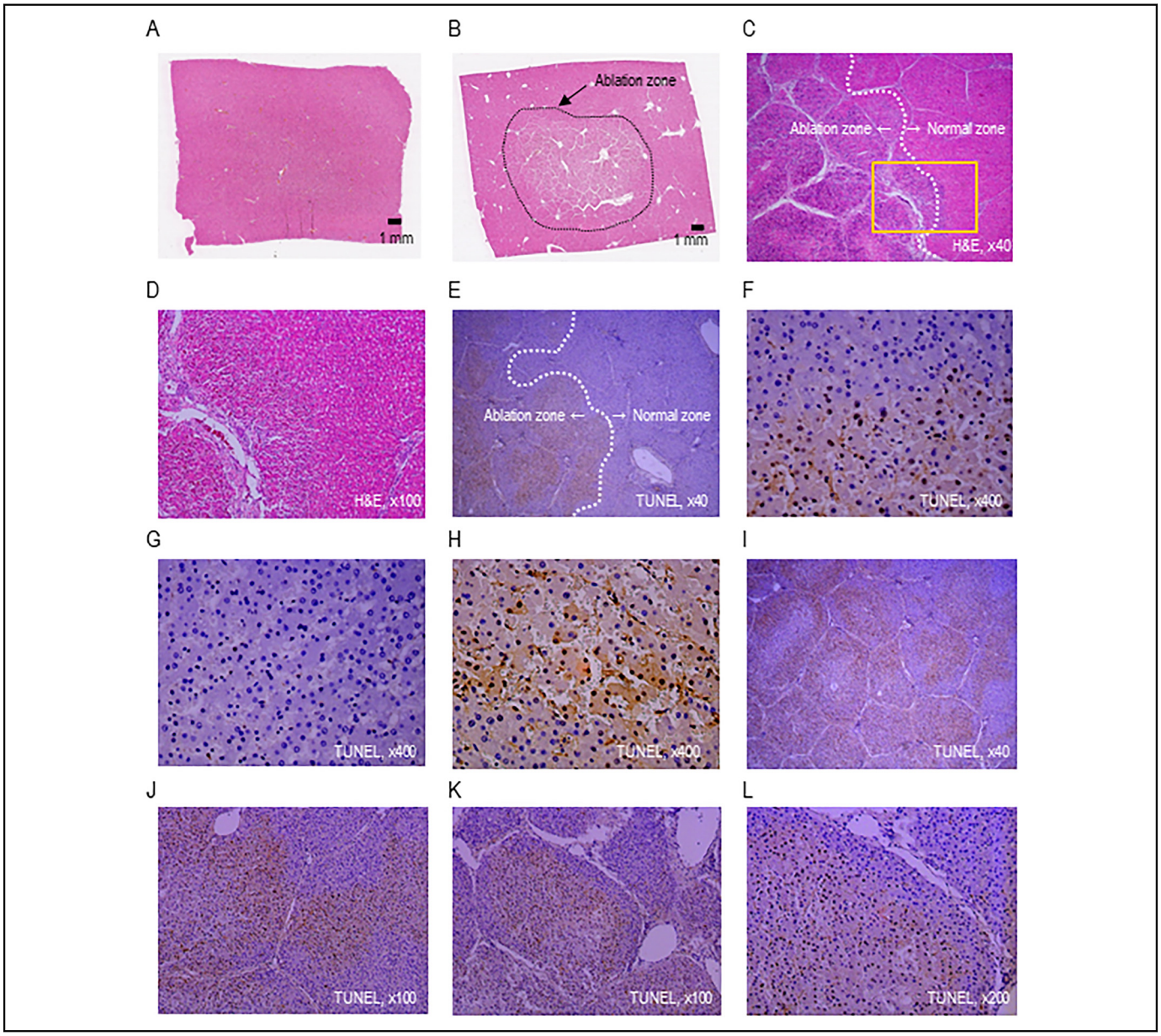

Figure 2. Microscopic view of the ablation boundary (A)–(F) and the distribution characteristics of apoptotic cells inside and between hepatic lobules after IRE application (G)–(I). (A) Whole slide H&E image of the untreated tissue. (B) Whole slide H&E image of the ablation zone (black dashed line) in the IRE-treated tissue. (C) Ablation boundary between the ablation zone and unaffected normal zone. (D) Magnified view of the yellow box in (E). (E) Ablation boundary in the IRE-treated tissue (F) Magnified view of the boundary between normal and apoptotic cells. (G) Live hepatocytes in the unaffected zone. (H) Apoptotic hepatocytes stained dark brown in the ablation zone. (I) Apoptotic area in the hepatic lobules of the ablation zone. (J) Distribution of apoptotic cells between two adjacent hepatic lobules after IRE (×100). (K) Distribution of apoptotic cells inside the hepatic lobule after IRE (×100). (L) Magnified view of image (M). The white dotted line indicates the ablation boundary.

significantly during IRE, but cardiac events such as serious arrhythmias or cardiac arrest did not occur.

The elliptic shape is a typical IRE ablation zone shape when two needle electrodes are used.[4] We have already observed the IRE ablation zone with 2,3,5-triphenyltetrazolium chloride (TTC) staining of IRE-treated liver tissue quickly and reliably. The livers of miniature pigs treated with needle-type IRE electrodes showed clear elliptical ablation zones after TTC staining (Supplementary Figure S1). In this study, IRE was performed under the same conditions as the previous experiment, and although the shape of the ablation zone was not determined by TTC staining, it was found that the basic shape of the IRE ablation zone was generally elliptical when using a needle electrode (Figure 1E and 1F, Table 2). After IRE treatment of 60 pulses rather than 90 pulses, the margin sharpness was less clear, but the surface ablation zone was larger. The IRE ablation zone was predicted to increase as the IRE pulse number increased, but such a trend could not be found only with the

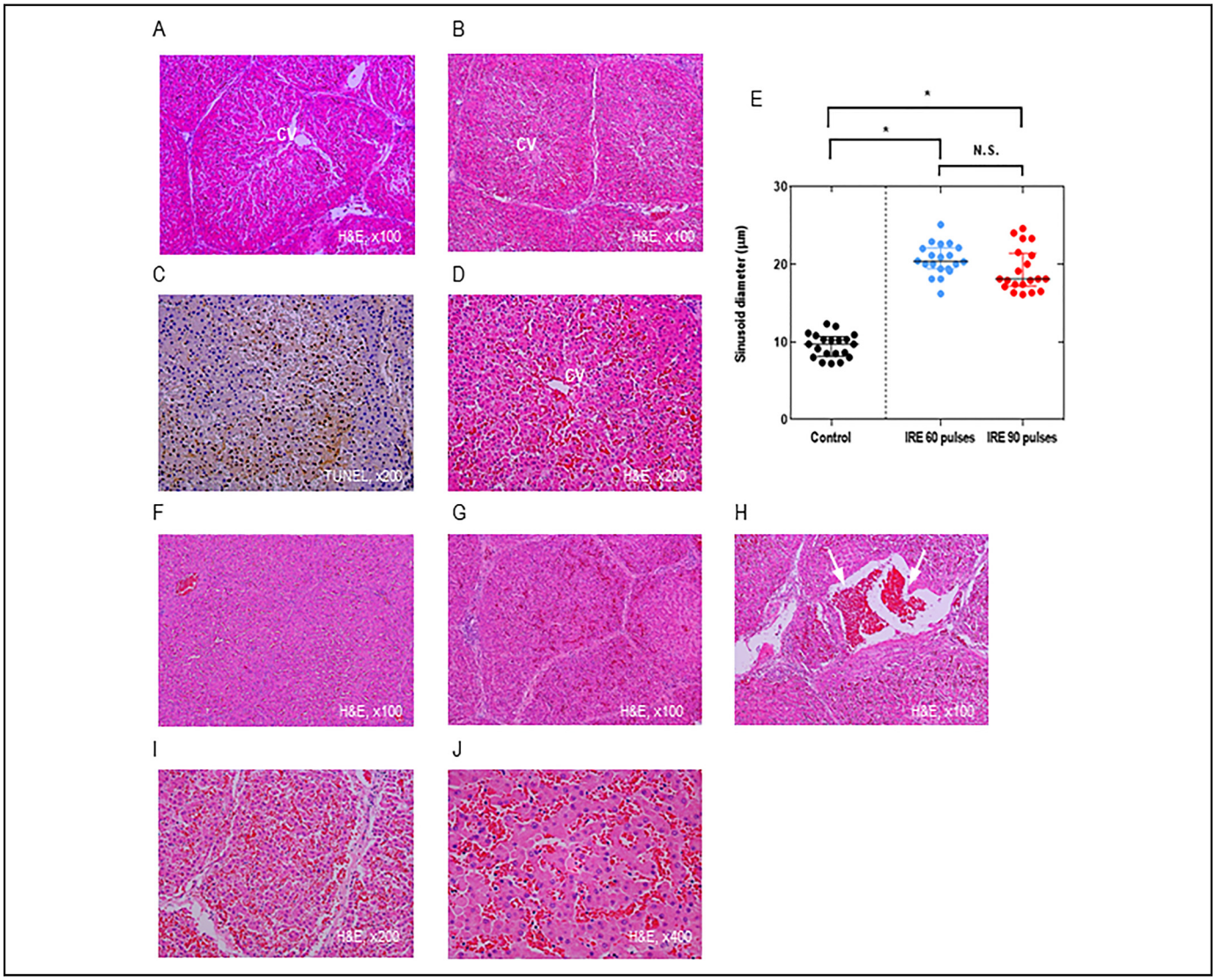

Figure 3. IRE-induced hepatic sinusoidal dilatation (A)–(E) and sinusoidal congestion after IRE application (F)–(I). (A) Dilated hepatic sinusoids are distributed radially around the central vein (CV) in the hepatic lobule after 60 pulses. (B) Dilatation of hepatic sinusoids after 90 pulses. (C) Dilated sinusoids in the apoptotic zone. (D) Dilated sinusoids filled with erythrocytes after IRE. (E) IRE-induced sinusoidal size changes. The asterisks (*) denote a significant difference compared to the untreated control (one-way ANOVA, $p < 0.05$, $n = 20$). N.S.; No significant difference between two groups. (F) Untreated hepatic parenchyma. (G) Congestion in the hepatic parenchyma after IRE. (H) Extensive congestion was observed in some hepatic parenchyma treated with 90 pulses. (I) Sinusoidal congestion after IRE. (J) Magnified view of hepatic sinusoids filled with erythrocytes after IRE. White arrows indicate the extensive congestive areas.

measurement values of the surface ablation zone reflecting only the lengths of the longest and shortest axes of the IRE ablation zone. The exact cause of this is unknown, but the possibility that such an effect may occur under certain IRE conditions cannot be completely ruled out. If the IRE pulses are continuously delivered to the same target point, as the pulse number increases, the electric field can be intensively distributed closer to the electrode insertion site rather than farther away. Therefore, the increase in IRE pulses may indicate the characteristic of forming an ablation zone with a clear boundary rather than an indefinite extension of the ablation zone with a faint boundary.

It is known that IRE has the advantage of complete ablation with well-demarcated boundaries.[14] However, although it is not a tumor tissue, a study also reported that viable and non-viable cells existed in the transition region when IRE (2700 V, 90 pulses, 100 μs) using a single bipolar electrode was applied to the liver of a normal pig.[20] To reduce such incomplete tissue ablation after IRE, it is necessary to closely examine the morphological changes of the ablation boundary according to the IRE input parameters in preclinical studies.

In this study, IRE was performed using two needle-type monopolar electrodes and only part of the IRE ablation boundary was partially clear, indicating that complete ablation was not

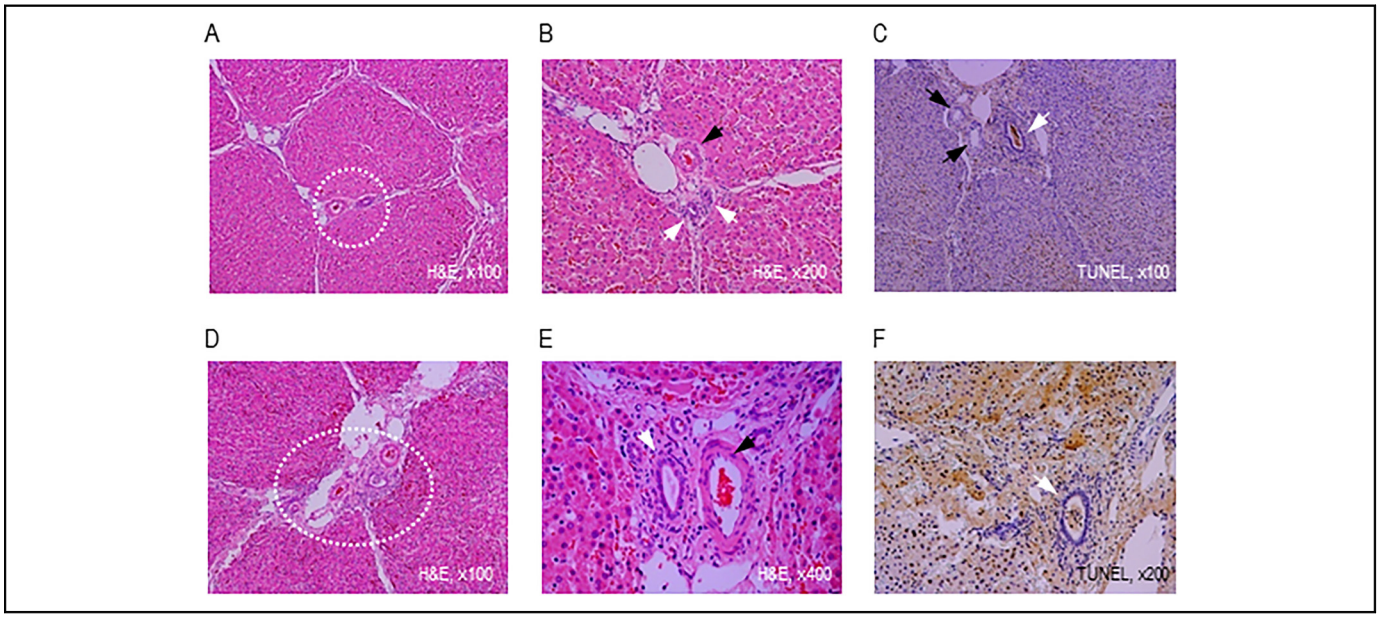

Figure 4. Intact preservation of tubular architectures in the IRE ablation zone treated with 60 pulses (A)–(C) or 90 pulses (D)–(F). (A) Tubular structures (white dotted circles) were observed in the hepatic parenchyma after IRE. (B) Magnified view of hepatic artery and bile ducts with well-preserved morphology. (C) Intact preservation of tubular architectures within the apoptotic area. (D) Preservation of tubular structures (white dotted circles) in the IRE-treated tissue. (E) Magnified view of the bile duct and hepatic artery with intact morphology. (F) Bile duct showing well-preserved shapes within the apoptotic area. The black arrows indicate the hepatic arteries, and the white arrows indicate the bile duct.

achieved (Figure 2). Histochemical staining analysis revealed that IRE ablation boundaries were formed mainly along the distribution lines of apoptotic cells within the hepatic lobular units, but not along the peripheral lines of the hepatic lobular units (Figure 2E). The unique hexagonal-like structures of hepatic lobule units remained intact even after IRE.

Apoptotic cells were distributed between adjacent hepatic lobules or slightly inward compared with the outermost margin of the hepatic lobule (Figure 2I and 2K). In addition to apoptosis, early lesion characteristics observed within 2 h after IRE treatment in the liver of animals are hepatic sinusoidal dilatation and congestion.[10] Sinusoidal congestion, an early sign of apoptosis or necrosis, can be observed at 1 h after IRE (electric field intensity of 1500 V/cm, a pulse length of 90 μs, 90 pulses) with a pair of needle electrodes in the liver of normal pigs.[11] In this study, in which similar IRE conditions were applied, sinusoidal congestion was observed in liver tissues of pigs collected within 2 h after IRE.

Dilated hepatic sinusoids were distributed radially around the central vein in the hepatic lobule after IRE pulse delivery. Compared to the untreated tissue, the sinusoid diameter was twice as wide in the IRE-treated tissue, and there was no significant difference between tissues treated with 60 and 90 pulses (Figure 2E). Erythrocytes infiltrated into dilated sinusoids, and extensive congestion was also observed in the hepatic parenchyma after 90 IRE pulses were applied (Figure 3G and 3J). Important vascular structures such as blood vessels and bile ducts are preserved after IRE.[6] In this study, we also observed that tubular structures such as hepatic arteries and bile ducts were preserved after IRE. In particular, the bile ducts of the IRE-treated tissues and the cells adjacent to the bile ducts were not stained dark brown by TUNEL staining (Figure 4C and 4F). These results indicate that the tubular structures were not damaged under the IRE conditions applied in this study (1500 V/cm, pulse length of 0.1 ms, 60 or 90 pulses, and electrode gap distance of 10 mm). The preservation of tubular structures after IRE has the potential to enhance antitumor effects by activating the immune system. IRE is known to activate lymphocytes in the blood and activate the immune system by maintaining an open state without causing occlusion of blood vessels by heat, unlike thermal ablation using radio frequency or microwaves.[4]

If there is an incompletely excised tumor tissue after IRE and the important structures such as blood vessels and lymphatic vessels are intact around it, the immune system will be activated and eventually induce apoptotic cell death of the remaining cancer cells. A report that systemic anti-tumor immune responses and long-term protective anti-tumor immunity were induced by IRE in a HCC-bearing small animal model provides further evidence that IRE activates the immune system.[12]

The histological changes induced by IRE in the liver of healthy pigs may be different from those of the tumor-forming liver. Despite these limitations, most preclinical studies related to IRE have used normal pigs because it is not easy to construct a large animal model with liver tumors. This study also has limitations in applying IRE ablation results of the normal liver to the tumor ablation. Nonetheless, the structure of pig liver is very similar to that of humans, so the results obtained in this study are expected to be a reference for investigating some characteristics of IRE-treated tumor tissues in human. In order to

further improve the therapeutic effect of IRE on gastrointestinal cancer in the future, it is necessary to identify various histological characteristics within the lesion using various image analysis techniques. Compared to RFA or MWA, tumor ablation such as IRE or electrochemotherapy shows various histological characteristics such as apoptosis, tissue generation, preservation of collagen matrix, preservation of blood vessels greater than 5 mm, and preservation of biliary structures.[21] It is difficult to evaluate the therapeutic effect of liver or pancreatic cancer only by reducing the size of the lesion, and it is recommended that it is more appropriate to analyze tumor viability using various image analysis techniques (eg, ultrasound imaging, magnetic resonance imaging, computed tomography, positron emission tomography, etc).[21]

Conclusions

A monophasic square wave pulse type of IRE was applied to porcine hepatic parenchyma using needle electrodes and induced a typical IRE ablation zone induced by the needle electrode. Furthermore, histological characteristics unique to IRE were observed in the initial ablation lesion of IRE, and the ablation effect was predicted through these results.

Acknowledgments

The authors would like to acknowledge Professor Su-Geun Yang, who is listed as the principal investigator in the ethics approval document. We also thank the entrusted institution (KNOTUS) staffs for assistance with animal vital sign monitoring and tissue sampling. We are grateful for the financial support of the National Research Foundation of Korea (Grant No. 2019M3E5D1A02069623, 2018R1A6A1A03025523, 2020R1A2B5B02002377 and 2021H1D 3A2A02045561)

Data Availability Statement

The data supporting this study are available on manuscript.

Declaration of Conflicting Interests

The author(s) declared no potential conflicts of interest with respect to the research, authorship, and/or publication of this article.

Ethical Approval

We submitted the animal experiment plan to KNOTUS, Co. Ltd (Non-clinical CRO, Korea), and entrusted animal testing under the approval of KNOTUS IACUC (Animal ethics approval number: KNOTUS IACUC: 21-KE-441). The principal investigator of this study is Professor Su-Geun Yang, and the director of the entrusted institution is listed in the ethics approval document. All experimental procedures were performed in accordance with animal ethics guidelines, and we tried to minimize the number of animals used and reduce pain during the treatment.

Funding

This work was financially supported by the Basic Science Research Program and Brain Pool program of the National Research Foundation (NRF) funded by the Korean government (MOE and MSIT) (RS-2023-00208587, 2018R1A6A1A03025523, and 2021H1D3A2A02045561) and the Young Medical-Scientist Research Grant Program funded by Daewoong Foundation (DFY2203P).

ORCID iD

Su-Geun Yang https://orcid.org/0000-0001-5278-8723

Supplemental Material

Supplemental material for this article is available online.

References

1. Zhou Y, Yang Y, Zhou B, et al. Challenges facing percutaneous ablation in the treatment of hepatocellular carcinoma: extension of ablation criteria. *J Hepatocell Carcinoma*. 2021;8:625-644. DOI: 10.2147/JHC.S298709.
2. Jiang C, Davalos RV, Bischof JC. A review of basic to clinical studies of irreversible electroporation therapy. *IEEE Trans Biomed Eng*. 2015;62(1):4-20. DOI: 10.1109/TBME.2014.2367543.
3. Vroomen L, Petre EN, Cornelis FH, et al. Irreversible electroporation and thermal ablation of tumors in the liver, lung, kidney and bone: what are the differences? *Diagn Interv Imaging*. 2017;98(9):609-617. DOI: 10.1016/j.diii.2017.07.007.
4. Hjouj M, Rubinsky B. Electroporation. In: Dupuy DE, Fong Y, McMullen WN, eds. *Image-Guided cancer therapy: a multidisciplinary approach*. Springer New York; 2013:21-36.
5. Vollherbst D, Bertheau RC, Fritz S, et al. Electrochemical effects after transarterial chemoembolization in combination with percutaneous irreversible electroporation: observations in an acute porcine liver model. *J Vasc Interv Radiol*. 2016;27(6):913-921.e2. DOI: 10.1016/j.jvir.2016.02.001.
6. Nault JC, Sutter O, Nahon P, et al. Percutaneous treatment of hepatocellular carcinoma: state of the art and innovations. *J Hepatol*. 2018;68(4):783-797. DOI: 10.1016/j.jhep.2017.10.004.
7. McBride S, Avazzadeh S, Wheatley AM, et al. Ablation modalities for therapeutic intervention in arrhythmia-related cardiovascular disease: focus on electroporation. *J Clin Med*. 2021;10(12):2657. DOI: 10.3390/jcm10122657.
8. Kielbik A, Szlasa W, Saczko J, et al. Electroporation-based treatments in urology. *Cancers (Basel)*. 2020;12(8):2208. DOI: 10.3390/cancers12082208.
9. Brock RM, Beitel-White N, Davalos RV, et al. Starting a fire without flame: the induction of cell eeath and inflammation in electroporation-based tumor ablation strategies. *Front Oncol*. 2020;10:1235. DOI: 10.3389/fonc.2020.01235.
10. Vogel JA, van Veldhuisen E, Agnass P, et al. Time-dependent impact of irreversible electroporation on pancreas, liver, blood vessels and nerves: a systematic review of experimental studies. *PLoS One*. 2016;11(11):e0166987. DOI: 10.1371/journal.pone.0166987.
11. Vogel JA, van Veldhuisen E, Alles LK, et al. Time-dependent impact of irreversible electroporation on pathology and ablation size in the porcine liver: a 24-h experimental study. *Technol Cancer Res Treat*. 2019;18:1533033819876899. DOI: 10.1177/1533033819876899.

12. Dai Z, Wang Z, Lei K, et al. Irreversible electroporation induces CD8(+) T cell immune response against post-ablation hepatocellular carcinoma growth. *Cancer Lett*. 2021;503:1-10. DOI: 10.1016/j.canlet.2021.01.001.
13. Gudvangen E, Kim V, Novickij V, et al. Electroporation and cell killing by milli-to nanosecond pulses and avoiding neuromuscular stimulation in cancer ablation. *Sci Rep*. 2022;12(1):1763. DOI: 10.1038/s41598-022-04868-x.
14. Lee EW, Thai S, Kee ST. Irreversible electroporation: a novel image-guided cancer therapy. *Gut Liver*. 2010;4(Suppl 1):S99-S104. DOI: 10.5009/gnl.2010.4.S1.S99.
15. Percie du Sert N, Hurst V, Ahluwalia A, et al. The ARRIVE guidelines 2.0: updated guidelines for reporting animal research. *Br J Pharmacol*. 2020;177(16):3617-3624. DOI: 10.1111/BPH.15193.
16. Zeng J, Qin Z, Zhou L, et al. Comparison between cryoablation and irreversible electroporation of rabbit livers at a location close to the gallbladder. *Radiol Oncol*. 2017;51(1):40-46. DOI: 10.1515/raon-2017-0003.
17. Sugimoto K, Kakimi K, Takeuchi H, et al. Irreversible electroporation versus radiofrequency ablation: comparison of systemic immune responses in patients with hepatocellular carcinoma. *J Vasc Interv Radiol*. 2019;30(6):845-853.e6. DOI: 10.1016/j.jvir.2019.03.002.
18. Sugimoto K, Moriyasu F, Kobayashi Y, et al. Assessment of various types of US findings after irreversible electroporation in porcine liver: comparison with radiofrequency ablation. *J Vasc Interv Radiol*. 2015;26(2):279-287. DOI: 10.1016/j.jvir.2014.11.007.
19. Zhu J-j, Bao J-l, Zhu C-y, et al. Cancer treatments of the irreversible electroporation. *Int J Clin Res Trials*. 2018;3:129. DOI: 10.15344/2456-8007/2018/129.
20. Cornelis FH, Durack JC, Kimm SY, et al. A comparative study of ablation boundary sharpness after percutaneous radiofrequency, cryo-, microwave, and irreversible electroporation ablation in normal swine liver and kidneys. *Cardiovasc Intervent Radiol*. 2017;40(1):1600-1608. DOI: 10.1007/s00270-017-169.
21. Granata V, Fusco R, Salati S, et al. A systematic review about imaging and histopathological findings for detecting and evaluating electroporation based treatments response. *Int J Environ Res Public Health*. 2021;18(11):5592. DOI: 10.3390/ijerph18115592.